ACS APPLIED MATERIALS & INTERFACES

RESEARCH ARTICLE

www.acsami.org

Boron-Assisted Transformation to Rod-Like Graphitic Carbons from Multi-Walled Carbon Nanotubes in Boron-Mixed Multi-Walled Carbon Nanotube Solids

Yoshinori Sato,*[,†,‡] Hikaru Nishizaka,[†] Kenichi Motomiya,[†] Go Yamamoto,[§] Akira Okubo,[⊥] Hisamichi Kimura,[⊥] Mikio Ishikuro,[⊥] Kazuaki Wagatsuma,[⊥] Toshiyuki Hashida,[§] and Kazuyuki Tohji[†]

[†]Graduate School of Environmental Studies, Tohoku University, Aoba 6-6-20, Aramaki, Aoba-ku, Sendai 980-8579, Japan

[‡]PRESTO, Japan Science and Technology Agency, Saitama 332-0012, Japan

[§]Fracture and Reliability Research Institute, Graduate School of Engineering, Tohoku University, Aoba 6-6-11, Aramaki, Aoba-ku, Sendai 980-8579, Japan

[⊥]Institute for Materials Research, Tohoku University, 2-2-1, Katahira, Aoba-ku, Sendai 980-8577, Japan

Supporting Information

ABSTRACT:

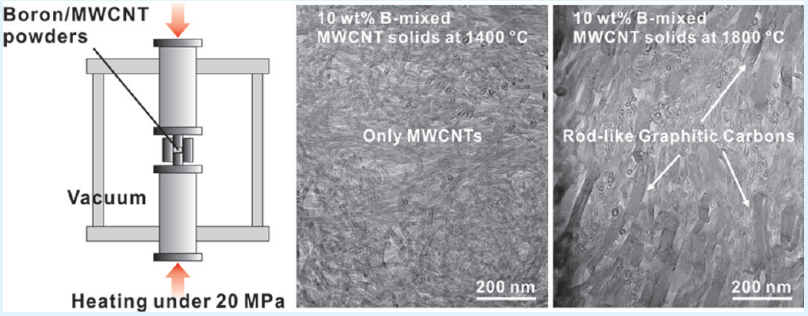

We produced boron-mixed multi-walled carbon nanotube solids (B-mixed MWCNT solids) by heating and pressing the powder of purified MWCNTs mixed with 1, 5, and 10 wt % boron in the temperature range 1400−1800 °C every 200 °C under a constant pressure of 20 MPa in vacuo, and investigated the influence of boron addition on nanotube structure and the mechanical and electrical properties of the resulting B-mixed MWCNT solids. The structure of the prepared material was characterized by scanning electron microscopy equipped with energy-dispersive X-ray spectroscopy, high-resolution transmission electron microscopy-electron energy loss spectroscopy, Raman scattering spectroscopy, and X-ray diffraction, and their mechanical properties and conductivity were measured using a mechanical and Vickers indentation tester and an electric resistor, respectively. It is notable that part of the nanotubes in the B-mixed MWCNT solids solidified at 1800 °C had dramatically changed into rod-like graphitic carbons (RLGCs). The occupancy distribution of RLGCs increased with increasing boron contents. However, boron was not detected in the energy-loss near-edge structure spectrum of RLGCs. Furthermore, RLGCs were not observed in the boron-unmixed sample treated with the same solidified condition, indicating that adding boron causes a remarkable ability to transform the phase of MWCNT. Transformation from MWCNTs to RLGCs resulted in increased specific bending strength and modulus, Vickers hardness, and electrical conductivity of B-mixed MWCNT solids with increasing boron content and solidified temperature.

KEYWORDS: carbon nanotubes, boron, solids, phase transition, rod-like graphitic carbons, boron carbide, mechanical properties, conductivity

INTRODUCTION

The development of strong composites with a lightweight material is needed in the energy field in an effort to achieve a fuel-efficient car and aircraft. The carbon nanotube (CNT) is a candidate for this lightweight material. However, one of the problems for this development is that CNTs cannot transfer the load to a matrix because of the slipping between the CNT and matrix. Highly graphitized multi-walled carbon nanotubes (MWCNTs) are chemically stable and hard to bond or fuse among themselves. Previously, we succeed in producing large-size binder-free MWCNT solids from fluorinated MWCNTs using a thermal heating and compression method in vacuum as one of the methods to obtain bonds between carbon nanotubes.[1] This technique resulted in the formation of covalent MWCNT

Received: March 16, 2011
Accepted: June 1, 2011
Published: June 01, 2011

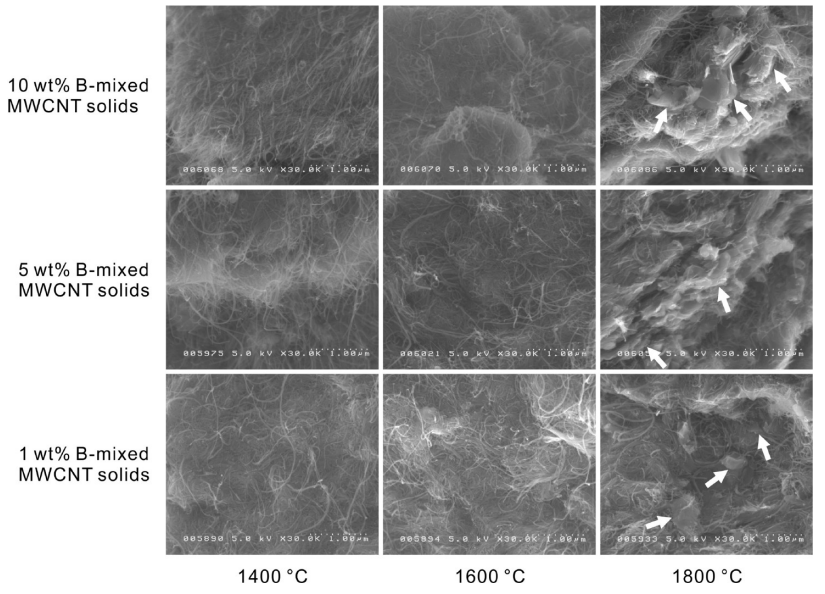

Figure 1. SEM photographs of a typical fracture cross-section of B-mixed MWCNT solids with each boron content at a given solidification temperature. White arrows show some bulkys observed in the B-mixed MWCNT solids solidified at a solidification temperature of 1800 °C.

networks generated by the introduction of sp^3-hybridized carbon atoms that cross-link between nanotubes upon de-fluorination. In contrast to this method, Endo et al. have studied the effect of boron on the structure of double-walled carbon nanotubes (DWCNTs) at high temperature under atmospheric pressure using argon gas.[2] They discovered some nanotube complexes by incorporation of boron, such as covalent nanotube "Y" junctions, DWCNT coalescence, and the formation of flat MWCNTs, and calculated from ab initio that the boron atom interstitials between DWCNTs play a role in establishing a covalent connection between neighboring nanotubes.

The boron atom enters the graphite lattice in the high temperature range of 1800 to 2350 °C, which results in a substitution in natural graphite with a maximum substitution of 2.35 at% (2.12 wt %) at 2350 °C in a vacuum.[3] Additionally, boron promotes the graphitization of carbon materials and acts as a sintering agent at a temperature of at least 2000 °C when the mixture of carbon materials and boron sources such as boron,[3,4] boron carbide (B_4C),[5,6] or boric acid (H_3BO_3)[7] is sintered by a heating and pressing treatment under atmospheric pressure using an inert gas. Endo's results are quite intriguing because DWCNTs reacted with boron to change into a new structure while keeping the nanotube within the moderate temperature range of 1400−800 °C, suggesting that the reactivity of the nanotube surface with a large curvature is higher than that of graphite[8,9] and that a moderate temperature prevents the DWCNT from undergoing phase transition to graphite under ordinary pressure. Given the application of an external pressure to CNT powders in order to increase the site of contiguous nanotubes, neighboring nanotubes might fuse and bond via the incorporation of boron to create new poly CNT structured materials.[10] Here, we prepared boron-mixed MWCNT solids ("boron-mixed MWCNT solids" are referred to as "B-mixed MWCNT solids") by heating purified MWCNT powders with 1, 5, and 10 wt % boron in the temperature range 1400 to 1800 °C every 200 °C under a constant pressure of 20 MPa in vacuo, and investigated the influence of boron addition on nanotube structure and the mechanical and electrical properties of the resulting B-mixed MWCNT solids. The structure of the prepared material was characterized by scanning electron microscopy (SEM) equipped with energy-dispersive X-ray spectroscopy (EDX), high-resolution transmission electron microscopy (HRTEM)-electron energy loss spectroscopy (EELS), Raman scattering spectroscopy, and X-ray diffraction, and their mechanical and electrical properties were measured using a mechanical and Vickers indentation tester and an electric resistor, respectively. It is notable that part of the nanotubes in the B-mixed MWCNT solids dramatically changed into rod-like graphitic carbons (RLGCs) under a pressure of 20 MPa and a moderate solidification temperature, and also that B_4C was produced in hthe solids. The occupancy distribution of RLGCs increased with increasing boron contents. However, the signal of boron K_{1s} was not detected in the EELS spectrum of RLGCs. Furthermore, RLGCs were not observed in the boron-free sample treated with the same solidified condition (MWCNT powders were not solidified in the absence of boron), indicating that the addition of boron causes a remarkable ability to transform the phase of the MWCNT. The bending strength and modulus, Vickers hardness, and electrical conductivity of the resulting solids increased with increasing boron content and solidified temperature. The B-mixed MWCNT solids solidified with high boron content and high temperature possessed slightly lower conductivity than those subjected to other solidification conditions, suggesting that synthesized B_4C with high resistivity increases in the solids.

EXPERIMENTAL SECTION

Purification of MWNTs. The purity of the MWCNTs was about 80 wt %, and the rest of the material consisted of amorphous carbon (8.50 wt %), Al (5.73 wt %), Fe (4.43 wt %), Mo (1.27 wt %), and Cr (0.07 wt %). The nanotubes exhibited tangle-like morphologies. The average tube diameter ranged from 20 to 40 nm, and the lengths were 500 nm to 5.0 μm. The MWCNT soot was burned in air at 500 °C for 90 min and the remaining soot was then introduced into a flask containing 6M-HCl in order to dissolve the Fe, Mo and Cr. Following this procedure, the acid solution was filtered using a membrane filter, and 1.0 g of the filtered material was transferred into a flask with 1.0 L of 2M-NaOH and refluxed at 100 °C for 6 h in order to dissolve the aluminum oxides. The resulting suspension was then filtered and washed with

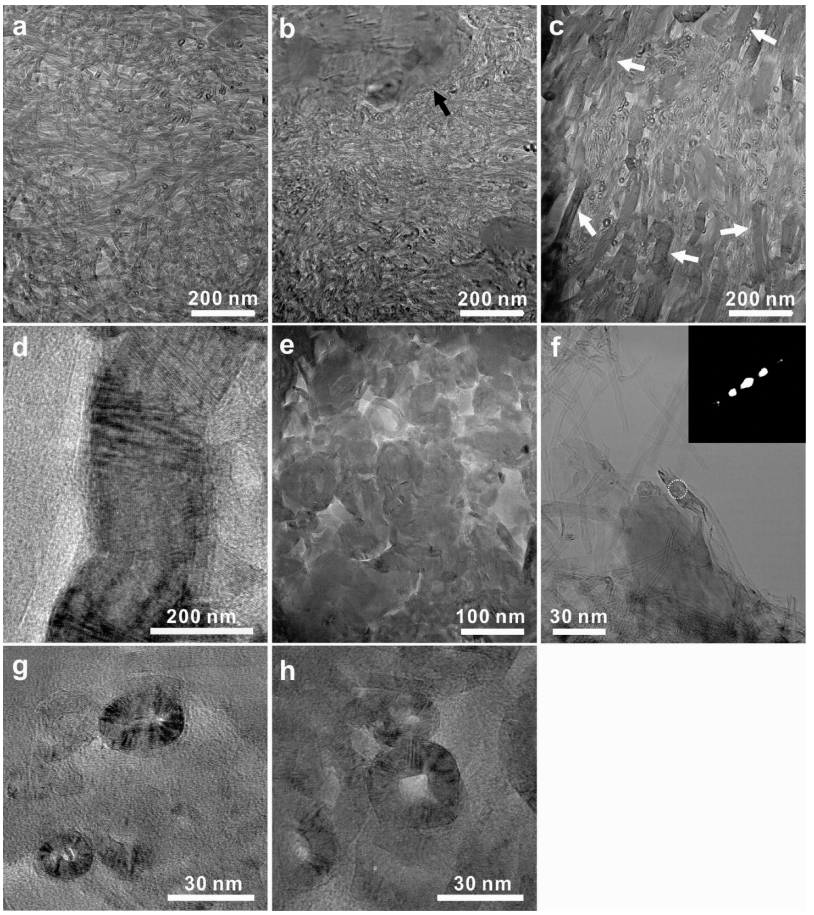

Figure 2. HRTEM image of a cross-section of 10 wt % B-mixed MWCNT solids at a solidification temperature of (a) 1400, (b) 1600, and (c) 1800 °C. Each solid was fabricated using a focused ion beam to observe a cross-section of the solids. Black arrow shows clusters in the solids solidified at 1600 °C (b). Many RLGCs existed in the 10 wt % B-mixed MWCNT solids solidified at 1800 °C (white arrow in c). (d) High-magnification HRTEM image of RLGCs and (e) HRTEM image of some clusters in the 10 wt % B-mixed MWCNT solids solidified at 1800 °C. (f) Inset is the electron diffraction of RLGC at the white-dotted circle in f. HRTEM images of a cross-section of the MWCNT observed in (g) 5 wt % and (h) 10 wt % B-mixed MWCNT solids.

hot water. Finally, samples were dried in vacuo at 200 °C for 24 h to evaporate water. After purification, the impurities consisted of Na (0.40 wt %), Al (1.41 wt %), Fe (0.26 wt %), Mo (1.27 wt %), and Cr (0.15 wt %), which were evaluated using inductively coupled plasma optical emission spectroscopy (ICP-OES; IRIS Advantage DUO, Thermo Fisher Scientific Co. Ltd., USA).

Production of B-Mixed MWCNT Solids. The boron-containing MWCNT powders were prepared by mixing an amorphous boron (Wako Pure Chemical Industries, Ltd., Japan) with the purified MWCNTs using an agate mortar by hand, in which each boron concentration for total mass was 1, 5, and 10 wt %. The B-mixed MWCNT solids were prepared using a spark plasma sintering (SPS) machine (Sumitomo Coal Mining, SPS-1050, Japan). Typically, 700 mg of the boron-containing MWCNT powders were used and hardened in a carbon-felt covered graphite die with a diameter of 20 mm and height of 60 mm at a given temperature ranging from 1400 to 1800 °C every 200 °C (heating rate: 25 K/min), under a pressure of 20 MPa in vacuo (1×10^{-2} Torr) for 10 min. The solidification temperature was measured using an irradiation thermometer. The average thickness of the resulting solids was 2.0 mm, which depended on the amounts of the set sample weight.

Characterization of B-Mixed MWCNT Solids. The sample morphologies were determined by scanning electron microscopy (SEM; S-4100, Hitachi, Japan) equipped with a field emission gun, which was operated at 5 kV. The SEM had an attached energy-dispersive X-ray detector (Genesis XM1, AMTEC Inc., USA) and the elemental analysis of the sample was detected at an accelerated voltage of 20 kV. In order to obtain information regarding nanotube structure in the B-mixed MWCNT solids by high-resolution transmission electron microscopy (HRTEM; HF-2000, Hitachi, Japan), we prepared a cross-section of solids with a rough thickness of 100 nm using a focused ion beam (FIB; FB-2000A, Hitachi, Japan). HRTEM equipped with a field emission gun was operated at 200 kV. In addition, we measured energy-loss near-edge structure (ELNES) spectra of cross-sectioned B-mixed MWCNT solids using a parallel EELS detector (GATAN GIF-2000) equipped with the HF-2000 in an effort to gather information concerning boron and carbon atoms in the solids. Raman scattering spectroscopy (Jobin-Yvon T64000, Horiba Co. Ltd., Japan) studies were used to analyze the vibrational modes of graphitic materials. The measurement was carried out at room temperature using an Ar ion laser with an excitation wavelength of 488.0 nm (Stellar-Pro-L, Modu-Laser, USA). The 002 spacing of carbon materials in the sample was evaluated using X-ray diffraction measurements. The resulting XRD profiles were corrected with reference to the report by Iwashita et al.[11] because the measured diffraction profiles broaden due to different intensity factors such as X-ray adsorption, as well as the Lorentz-polarization factor and atomic scattering factor. Additionally, an internal standard Si must be mixed in the sample in order to avoid the shifting and broadening of diffraction peaks due to the performance of the XRD diffractometer employed in the analysis.

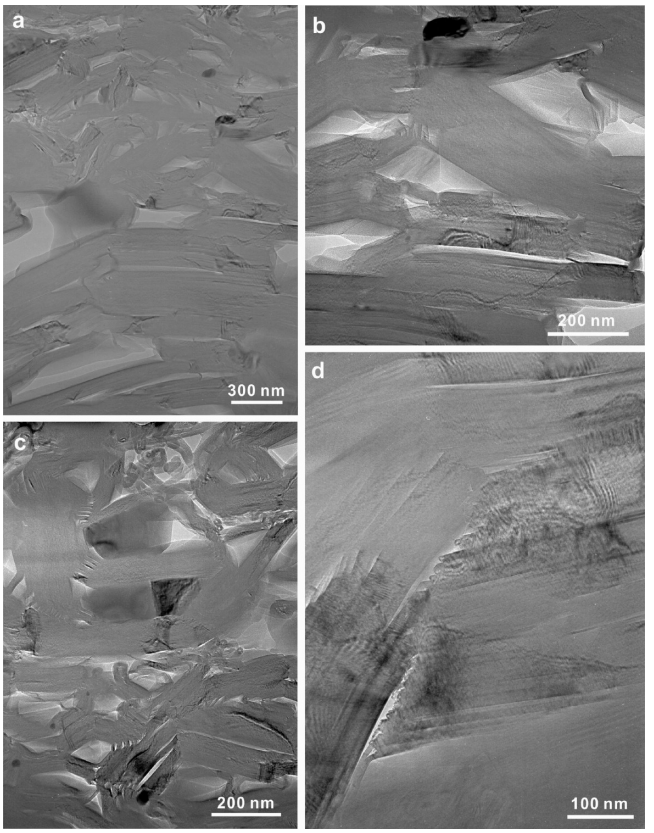

Figure 3. Typical HRTEM images of the assembly of RLGCs. (a−c) Low-magnification HRTEM images of RLGCs. There are pores resulting from the assembly of RLGCs. (d) High-magnification HRTEM image of the RLGCs.

Chemical Analysis of the Boron Content in B-Mixed MWCNT Solids. Separation and determination of boron such as amorphous boron, boron substituted in the MWCNTs, and B_4C in the B-mixed MWCNT solids were conducted as follows. Amorphous boron was dissolved with 7N HNO_3.[12] B_4C was not dissolved with 7N HNO_3, but dissolved with molten sodium carbonate.[13] In addition, boron substituted in the MWCNTs was not dissolved with molten sodium carbonate.[6] The pulverized sample was dissolved with molten sodium carbonate in a platinum crucible to remove boron substituted in the MWCNTs. The cake in the crucible was dissolved with distilled water. After filtration, the insoluble residues on filter paper were transferred into the platinum crucible. The insoluble residual such as boron substituted in the MWCNTs was suspended in a 3 wt % solution of $Ca(OH)_2$, and was then ignited at about 900 °C. The residue in the platinum crucible was dissolved with 7N HNO_3. The amounts of boron in the separated insoluble residue (boron as substituted in the MWCNTs) and filtrate (boron as B_4C) were determined by inductively coupled plasma-optical emission spectrometry (ICP-OES; IRIS Advantage DUO, Thermo Fisher Scientific Co. Ltd., USA). The pulverized sample was dissolved with 7N HNO_3 to remove B_4C. After filtration, the amounts of boron in the separated insoluble residue (boron as B_4C) and filtrate (boron as amorphous boron) were determined by ICP-OES.

Bulk Density Measurements. All specimens were shaped into rectangular pieces ($2.0 \times 1.0 \times 10$ mm^3). The specimens were polished as described above. The bulk densities of the solids were measured using an analytical electrobalance (GR-202; A & D Co. Ltd., Japan) and a high-precision microscale (M200; Mitutoyo Co., Japan) for length, width, and thickness determinations.

Mechanical Properties. The mechanical properties of the solid blocks, Young's modulus, and fracture strength were measured using

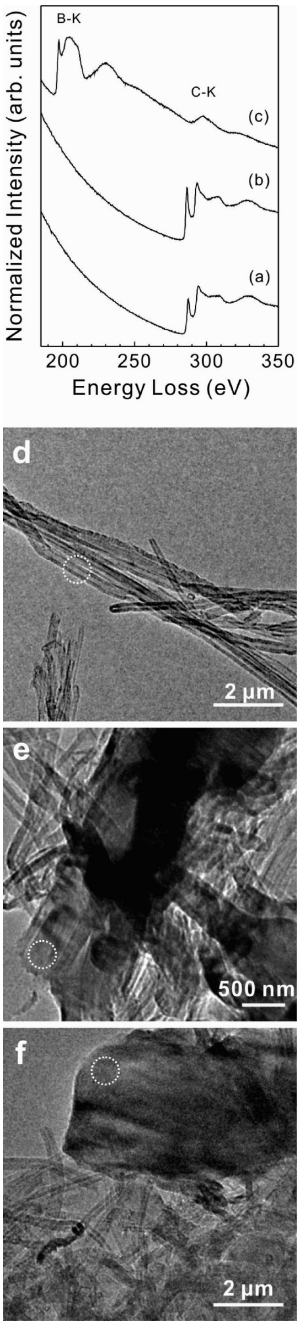

Figure 4. Typical ELNES spectrum of (a) MWCNTs, (b) RLGCs, and (c) clusters in 10 wt % B-mixed MWCNT solids solidified at 1800 °C. HRTEM images of (d) MWCNTs, (e) RLGCs, and (f) clusters in which the white-dotted circle represents the measured area of each material.

three-point bending tests, which were performed on a universal testing machine (Instron 5582) at atmospheric conditions and room temperature. The load was applied at a crosshead speed of 0.05 mm/min. Young's modulus Eb and fracture strength σb are given by the following equations

$$E_b = 1/4(L^3/bh^3)P/\delta, \sigma_b = (3P_bL/2bh^2)$$

where L is the span length (16 mm), b the specimen width (2.0 mm), h the specimen thickness (1 mm), P/δ the initial linear slope of the load versus load-line displacement curve, and P_b the maximum load. Three specimens were tested, and averaged results were calculated. The shape

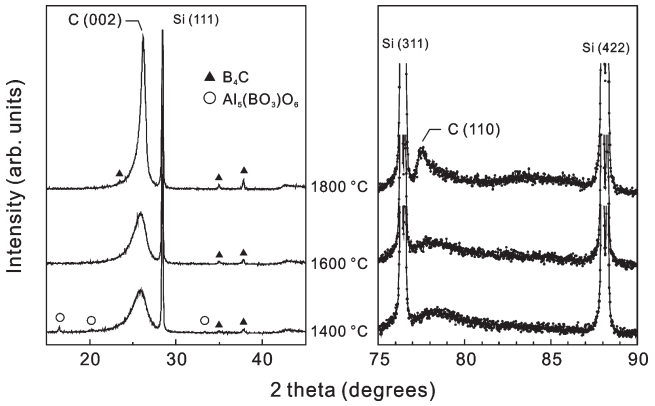

Figure 5. XRD profile of 10 wt % B-mixed MWCNT solids at three solidification temperatures.

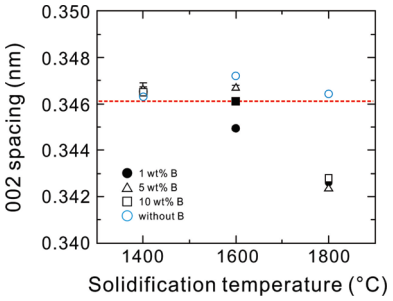

Figure 6. 002 lattice spacing of B-mixed MWCNT solids plotted against solidification temperature. Blue circles show the lattice spacing of B-unmixed MWCNTs treated under the same conditions for solidification. Red-dashed line is the 002 lattice spacing of the starting MWCNTs.

of tested specimens was approximately 2.0 × 1.0 × 18 mm^3. The solid specimens were polished with Emery paper (# 1000) and Fuji film lapping tape (# 2000 and # 4000) (Fuji Photo Film Co., Ltd., Japan). After the samples were polished, they were sonicated in ethanol for 5 min and dried at 100 °C for 24 h. Six tests were performed on each material.

Indentation tests were carried out on a HMV-1/2 hardness tester with a diamond Vickers indenter (SHIMAZU Co. Ltd., Japan). The indentation parameters included a load of 1.961 N with a dwell of 15 s. Vickers indentation sites were observed by SEM. Ten tests were performed on each material.

Electrical Conductivity Measurements. The specimens were measured at room temperature on rectangular blocks (2.0 × 1.0 × 18 mm) parallel to their long axis, i.e., perpendicular to the pressing axis. The solid specimens were polished as mentioned above. The electrical conductivity of the solids was measured using a Four-probe method (Loresta GP; Dia Instruments Co., Ltd., Japan), which was measured by holding an Au pin electrode against the sample surface (Four-probe method recorded at room temperature, in which each pin-electrode was deposited every 2.0 mm). Volume resistivity was calculated by multiplying resistance by the resistivity correction factor (RCF), determined according to the sample's shape and size. Note that conductivity is the inverse of volume resistivity.

RESULTS AND DISCUSSION

All of the solids consisted of many needle-like materials as observed from SEM photographs of a typical fracture cross-section of B-mixed MWCNT solids with each boron content at a given solidification temperature (Figure 1), and some agglomerates were observed in B-mixed MWCNT solids solidified at a solidification temperature of 1800 °C (white arrow in Figure 1). The HRTEM image of a cross-section of 10 wt % boron-mixed MWCNT solids ("10 wt % boron-mixed MWCNT solids" are referred to as "10 wt % B-mixed MWCNT solids"; 1 wt % boron- and 5 wt % boron-mixed MWCNT solids are also referred to in the same manner) which were fabricated using a focused ion beam revealed that solids solidified at 1400 °C mostly consisted of MWCNTs (Figure 2a). In the case of the solids solidified at 1600 °C, a few clusters were observed other than MWCNTs (black arrow in Figure 2b). It is striking that many RLGCs (white arrow in Figure 2c and high-magnification HRTEM image in Figure 2d) were present in the 10 wt % B-mixed MWCNT solids solidified at 1800 °C, with a few MWCNTs and clusters (Figure 2e), and some RLGCs were also synthesized in the 1 and 5 wt % B-mixed MWCNT solids solidified at 1800 °C (see Figure S1 in the Supporting Information). The diameter of RLGCs was in the range 20 to 100 nm (Figures 2c and 2d), and the average 002 spacing of RLGC was estimated as 0.347 nm (standard deviation: ± 0.001 nm) from the electron diffraction of RLGC (inset in Figure 2f) at the white-dotted circle in Figure 2f. The cross-section of the MWCNT observed in these solids showed an ellipsoidal shape (Figure 2g) and two nanotubes exhibited a tight contact at the outside layer (Figure 2h), an effect of the solidification pressure. Figure 3 shows some typical HRTEM images of the RLGC assembly. The 002 lattice image of RLGCs is parallel to the axis (Figure 3a,c), showing that MWCNTs were transformed into a rod-like shape. As shown in Figure 3b,c, the solids had many pores, which indicated that the assembled RLGCs were not in tight contact with each other, corresponding with the bulk density of B-mixed MWCNT solids which was smaller than that of natural graphite (2.2 g/cm^3) as discussed later in this study. By contrast, RLGCs were not observed in B-unmixed MWCNTs treated under the same conditions for solidification (see Figure S2 in the Supporting Information), indicating that adding boron dramatically causes nanotube phase-transformation to graphitic carbon under conditions of 20 MPa and 1800 °C.

Energy-loss near-edge structure (ELNES) in an EELS spectrum provides information on the structural and chemical composition of the sample. The boron K_{1s} excitation edge exhibits $1s \rightarrow \sigma^*$ and $1s \rightarrow \pi^*$ excitations with the same position as for boron in an sp^2 bonded environment. The position of the main π^* resonance at 192 eV is typical for hexagonal boron nitride (BN) and multi-walled BN nanotubes,[14] which is proof that the boron possesses chemical bonding with sp^2 hybridization. Figure 4 shows each typical ELNES spectrum of (a) MWCNTs, (b) RLGCs, and (c) a cluster in the 10 wt % B-mixed MWCNT solids solidified at 1800 °C. The measured area of each material is the white-dotted circle as shown in Figures 4d ~ 4f. There is no peak around 192 eV in each ELNES spectrum of both RLGCs and MWCNTs, but there is a peak around 284 eV which comes from the C K_{1s} excitation edge ($1s \rightarrow \pi^*$) for graphitic carbon. On the other hand, the ELNES spectrum of the cluster is similar to that of boron carbide (B_4C).[15] Curiously, boron atoms cannot be detected in the RLGCs. Actually, we estimated boron contents in the B-mixed MWCNT solids according to the chemical method to dissolve the substituted boron into graphite (see the Experimental Section). We could not estimate the content of boron atoms from the substituted boron in the sample, but detected the boron dissolved

Table 1. 002 spacing, *R* values, and L_a of B-Mixed MWCNT Solids

boron content (wt %)	SPS temp (°C)	solidification	002 spacing (nm)	D-band (cm^{-1})	G-band (cm^{-1})	G′-band (cm^{-1})	*R* value (I_D/I_G)	L_a (nm)
0			0.3462	1358.7	1584.6	1622.5	0.65	6.79
0	1400	no	0.3463	1358.8	1584.4	1623.4	0.55	8.03
	1600	no	0.3472	1359.3	1583.8	1623.8	0.50	8.80
	1800	no	0.3464	1359.4	1583.0	1624.5	0.41	10.67
1	1400	yes	0.3466	1358.9	1585.3	1621.4	0.71	6.18
	1600	yes	0.3450	1361.9	1590.0	1618.1	0.89	4.93
	1800	yes	0.3426	1361.5	1590.3	1618.0	0.91	4.86
5	1400	yes	0.3466	1358.7	1584.9	1622.0	0.69	6.38
	1600	yes	0.3467	1361.5	1589.8	1620.5	0.90	4.90
	1800	yes	0.3424	1363.1	1589.7	1618.2	0.86	5.13
10	1400	yes	0.3465	1359.4	1584.9	1622.0	0.69	6.35
	1600	yes	0.3461	1361.2	1590.7	1619.5	0.88	4.97
	1800	yes	0.3428	1361.5	1590.2	1618.2	0.85	5.18

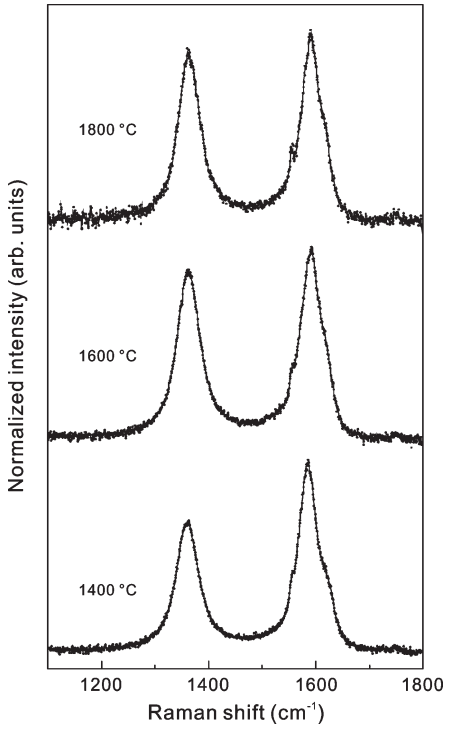

Figure 7. Raman scattering spectra of 10 wt % B-mixed MWCNT solids at three solidification temperatures.

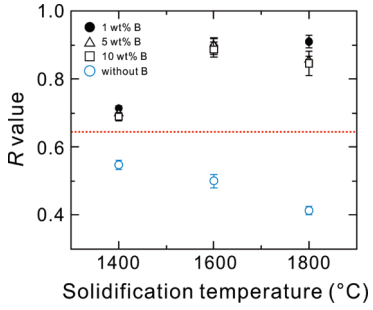

Figure 8. Intensity ratio I_D/I_G (*R* value) of B-mixed MWCNT solids plotted against solidification temperature. Red circles show the intensity ratio of B-unmixed MWCNTs treated under the same conditions for solidification. Red-dashed line is the intensity ratio *R* of the starting MWCNTs.

in HNO_3. Additionally, we could estimate non-dissolved boron compounds in HNO_3 such as B_4C (Table S1 in the Supporting Information). The detection of boron using HRTEM-EELS depends on the boron concentration in the material. McGuire et al. have noted that the detection limit of the nano-EELS instrument is 0.05−0.1 at % boron.[16] If any boron is indeed substituted in RLGC, it will be below this limit. Thus, we cannot necessarily conclude that no boron exists in the carbon network of RLGCs on the basis of HRTEM-EELS, and therefore we used XRD and Raman scattering measurements to investigate the effect of boron addition on the structural change of CNT in the B-mixed MWCNT solids.

The XRD profile of 10 wt % B-mixed MWCNT solids at three solidification temperatures are shown in Figure 5, and the 002 lattice spacing of B-mixed MWCNT solids plotted against solidification temperature is presented in Figure 6. A diffraction line range from 25.90−26.21° comes from the 002 lattice spacing derived from graphitic materials. The B-unmixed MWCNTs treated under the same conditions for solidification have a 002 lattice spacing of 0.346 nm, indicating that the spacing did not shrink in comparison to that of the starting materials (see Table 1 and blue circle in Figure 6). Additionally, they did not show the 110 diffraction line. The XRD profiles of 10 wt % B-mixed MWCNT solids solidified at 1400 °C showed several peaks at 16.46, 20.30, 33.32, 35.10, and 37.84°, thought to correspond to the diffraction lines of aluminum oxide borate ($Al_5(BO_3)O_6$)[17] and B_4C.[17] Boron is thought to react with the residue of aluminum oxide, which was present with the purified MWCNTs (see Experimental Section; the impurity concentration of the aluminum atom was 1.4 wt %). The XRD profiles of B-mixed MWCNT solids solidified at 1600 or 1800 °C showed two peaks at 35.10 and 37.84°, corresponding to the diffraction lines of the (104) and (021) plane of rhombohedral B_4C. This pattern was the same as the behavior of XRD profiles of 1 and 5 wt % B-mixed MWCNT solids.

Surprisingly, it was noted that B_4C had already been synthesized at a solidification temperature of 1400 °C. But why was B_4C synthesized at a relatively low temperature of 1400 °C? The

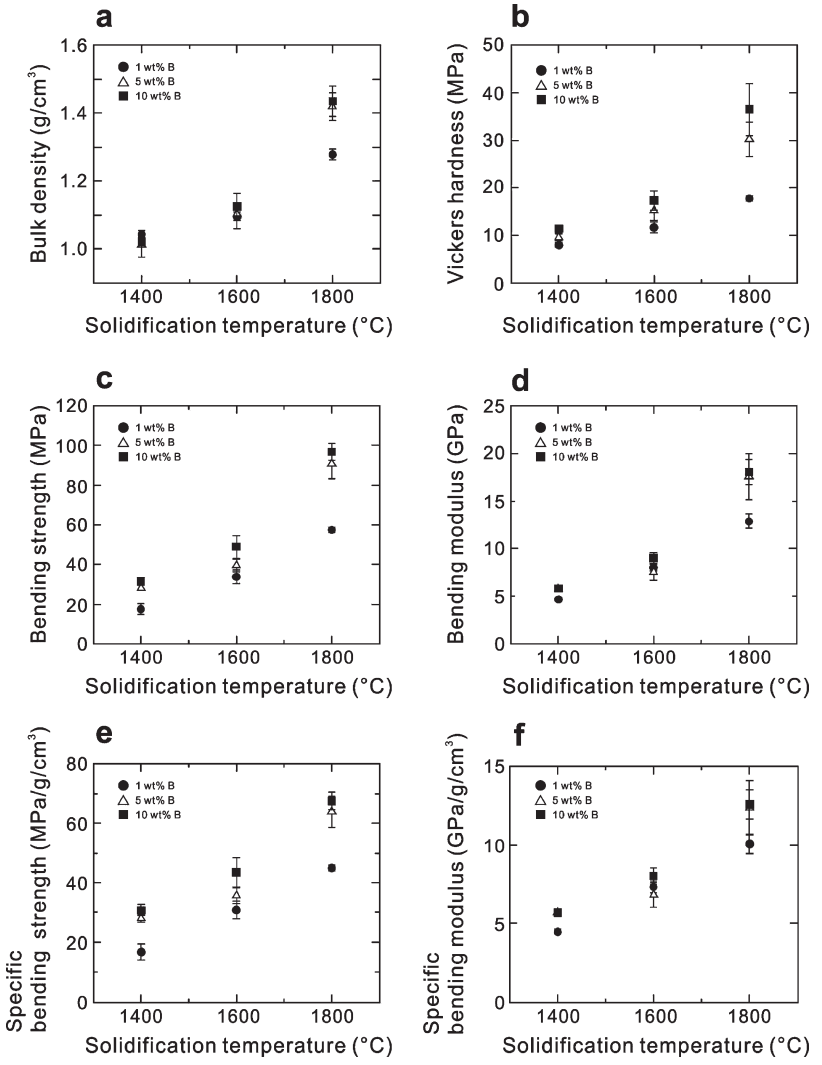

Figure 9. Mechanical properties of B-mixed MWCNT solids. (a) Bulk density, (b) Vickers hardness, (c) bending strength, (d) bending modulus, (e) specific bending strength, and (f) specific bending modulus.

reason seems to be that the carbon atom of the CNT with a high curvature is under a high reactive condition because of the CNT being compacted by the solidification pressure. An additional reason seems to be that the lack of uniformity of the boron atom in the MWCNT powder before solidification makes it easy for it to form B_4C, and hence results in a high concentration of boron that forms B_4C. Another reason seems to be the solidification process using SPS. The SPS systems involve a unique synthesis and processing technique, which makes possible the sintering of particles at low temperatures and for short periods of time by charging particles with electrical energy, and effectively applies the high energy of a spark plasma. The SPS process experiences a very high thermal efficiency because of the direct heating caused by the spark. In the case of the above-mentioned situation, CNTs react with boron to synthesize B_4C due to the high temperature because of a local spark. The diffraction integral intensity of the 002 spacing of graphite dramatically increased and their lattice spacing narrowed with increasing solidification temperature (see Table 1 and Figure 6). On the other hand, the 110 diffraction line of the graphitic materials clearly appeared in only the B-mixed MWCNT solids solidified at a solidification temperature of 1800 °C. Combined with the HRTEM observation, the increase in integral intensity of the 002 diffraction line, shrinking of the 002 lattice spacing, and appearance of the 110 diffraction line in only the B-mixed MWCNT solids solidified at 1800 °C support the occurrence of a transition from many MWCNTs to RLGCs. In the analysis using XRD, we can not evaluate the substitution of boron atoms into MWCNTs and RLGCs.

Raman scattering spectra of 10 wt % B-mixed MWCNT solids at three solidification temperatures are shown in Figure 7, and the intensity ratio I_D/I_G (R value) of B-mixed MWCNT solids plotted against solidification temperature is presented Figure 8. The Raman scattering spectrum showed a pair of bands around 1360 cm^{-1} (D-band) and 1590 cm^{-1} (G-band). Additionally, a band appeared at around 1620 cm^{-1} (D′-band) derived from a vibration mode of a disordered carbon network, which was stronger with increasing intensity of the D-band.[18−21] The R value is known to depend on the number of defects in the nanotubes.[2] The R values of B-unmixed MWCNTs treated under the same conditions for solidification decreased with increasing solidification temperature (Table 1 and blue circle in Figure 8). This indicates that the crystallite of the nanotube network was

Table 2. Physical Properties of B-Mixed MWCNT Solids

boron content (wt%)	SPS temp. (⊠C)	bulk density (g/cm^3)	bending strength (MPa)	bending modulus (GPa)	specific bending strength (MPa/g/cm^3)	specific bending modulus (GPa/g/cm^3)	Vickers hardness (MPa)	electrical conductivity (S/cm)
1	1400	1.04	17.5	4.7	16.7	4.5	8.0	190.3
	1600	1.10	33.8	8.0	30.8	7.3	11.7	406.8
	1800	1.28	57.4	12.9	44.9	10.1	17.7	657.6
5	1400	1.01	28.3	5.7	28.0	5.7	9.7	178.3
	1600	1.10	39.4	7.5	35.7	6.8	15.3	397.3
	1800	1.42	90.6	17.6	63.8	12.4	30.2	740.8
10	1400	1.02	31.4	5.8	30.7	5.7	11.4	166.8
	1600	1.12	48.9	9.0	43.5	8.0	17.3	374.4
	1800	1.43	96.8	18.0	67.5	12.6	36.5	601.3
IG-11	-	1.74	39.0	9.8	22.4	5.6	16.8	600.0

rearranged to result in the high graphitization of MWCNTs, which accords with the XRD data. On the other hand, with increasing solidification temperature the D- and G-band shifted to a higher wavenumber, and the intensity of the D- and D′-band were stronger and the *R* value increased. This phenomenon occurs when boron atoms are substituted into the network frame of carbon.[22,23] The *R* value had already increased at a solidification temperature of 1400 °C, indicating that boron interacts with the nanotubes. Additionally, when boron atoms are substituted into the network of graphite, the distance between the substituted boron atoms can be estimated as a crystallite diameter (L_a),[7] which is expressed according to the following formula using the *R* value:[18] $L_a = 44/R$. According to a previous report,[7] as the number of substituted boron atoms increases, L_a decreases. In the case of this study, the L_a value of the purified MWCNTs was 6.79, and L_a of B-unmixed MWCNTs treated under the same conditions for solidification increased with increasing solidification temperature (Table 1), indicating that the in-plane of graphene was developed. On the other hand, L_a of B-mixed MWCNT solids decreased with increasing solidification temperature, indicating the possibility of the substitution of boron into the framework of CNTs. In comparison with the XRD analysis, Raman scattering spectroscopy provides information on the vibration between atoms and is very sensitive to any defective vibration of the carbon framework. Our Raman data showed that the interaction of boron and CNTs begins to occur at 1400 °C.

The signal of boron could not be detected in the EELS of RLGC, but MWCNTs were considered to react with boron as shown in Raman spectra. In contrast, RLGCs were not observed in the boron-unmixed sample, indicating that boron prompts the formation of RLGCs. Is boron substituted in the lattice of RLGC? Hishiyama et al. reported that 2 wt % boron was doped in a graphite film when a graphite film sandwiched with two 10 wt % boron-containing carbon plates was annealed by two-step heating in the range 2350 to 2500 °C for several minutes under vacuum, revealing that boron was able to diffuse into the carbon materials by the physical contact.[23] Regarding our study, a small amount of boron might be diffused into the MWCNTs and transformed to the RLGC by the effects of the high reactivity of the curvatured-nanotube surface and application of pressure, even when the temperature was in the range 1400−1800 °C.

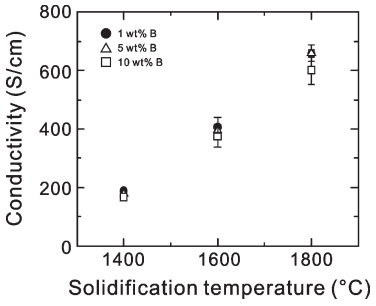

Figure 10. Conductivity of B-mixed MWCNT solids.

The bulk density of the B-mixed MWCNT solids increased with increasing solidification temperature at each concentration of boron (see Figure 9a and Table 2), which supports the structure change from MWCNTs to RLGCs or B_4C. In solids solidified at 1400 °C, the bulk density of all B-mixed MWCNT solids was almost the same, indicating that the effect of boron addition on the structure of MWCNTs does not appear because the temperature for the boron atom to react with MWCNT is low. Figure 9b−f shows estimates of Vickers hardness, bending strength, and bending modulus of the B-mixed MWCNT solids and their specific bending strength and bending modulus (see Table 2). Vickers hardness, bending strength, and modulus of the B-mixed MWCNT solids increased with increasing solidification temperature. The specific bending strength and bending modulus of the B-mixed MWCNT solids, except the 1 wt % B-mixed MWCNT solids solidified at 1400 °C, were much higher than those of commercial graphite IG-11 (specific bending strength: 22.7 MPa/g/cm^3; specific bending modulus: 5.6 GPa/g/cm^3). The mechanical properties of B-mixed MWCNT solids were augmented with a solidification temperature of 1600 °C, which was expected if considering that the transformed carbon materials such as RLGCs and B_4C have improved strength and hardness. The conductivity of the B-mixed MWCNT solids gradually increased following increased solidification temperature (Figure 10). The conductive routes are considered to increase not by the substitution of boron into MWCNTs and RLGCs, but by the densification of the solids. With increasing boron content at a constant solidification temperature,

the conductivity becomes slightly lower, which might be caused by the B_4C produced in the solids. The sintered B_4C solids had a conductivity of 2.0−20 S/cm, which is a tenth or hundredth times lower than that of de-fluorinated MWCNT blocks or commercial graphite.[1]

The B-mixed MWCNT solids in this study possessed lightweight and high mechanical properties relative to those of conventional graphites and carbon materials, which is very promising for application as a structural material or an electrode. In the B-mixed solids, some boron atoms reacted with MWCNTs to produce B_4C. Therefore, ^{10}B-mixed MWCNT solids including isotope boron (^{10}B), which absorbs neutrons, are expected to be used as material for a nuclear fission reactor or neutron absorber.

CONCLUDING REMARKS

We produced B-mixed MWCNT solids by heating and pressing the powder of purified MWCNTs mixed with 1, 5, and 10 wt % boron in the temperature range 1400 to 1800 °C every 200 °C under a constant pressure of 20 MPa in vacuo, and investigated the influence of boron addition on nanotube structure and the mechanical and electrical properties of the resulting B-mixed MWCNT solids. It is notable that part of the nanotubes in the B-mixed MWCNT solids solidified at 1800 °C and dramatically changed into RLGCs. The occupancy distribution of RLGCs and B_4C increased with increasing boron contents. However, boron was not detected in the EELS spectrum of RLGCs. On the other hand, RLGCs were not observed in the boron-unmixed sample treated under the same solidified conditions, indicating that adding boron causes a remarkable ability to transform the phase of the MWCNT. Transformed RLGCs from MWCNTs, the specific bending strength and modulus, Vickers hardness, and electrical conductivity of the B-mixed MWCNT solids increased with increasing boron content and solidified temperature, and they also possessed a slightly lower conductivity than those materials under other solidification conditions, suggesting that synthesized B_4C with a high resistivity increases in the solids.

ASSOCIATED CONTENT

Supporting Information. HRTEM image of a cross-section of 1 and 5 wt % B-mixed MWCNT solids at a solidification temperature of 1800 °C (Figure S1); HRTEM images of B-unmixed MWCNTs treated under the same conditions for solidification (Figure S2); chemical analysis of boron content (Table S1). This material is available free of charge via the Internet at http://pubs.acs.org.

AUTHOR INFORMATION

Corresponding Author
*E-mail: hige@bucky1.kankyou.tohoku.ac.jp. TEL & FAX: +81-22-795-3215.

ACKNOWLEDGMENT

This work was supported by PRESTO-JST from the Ministry of Education, Science, Culture and Sport of Japan.

REFERENCES

(1) Sato, Y.; Ootsubo, M.; Yamamoto, G.; Van Lier, G.; Terrones, M.; Hashiguchi, S.; Kimura, H.; Okubo, A.; Motomiya, K.; Jeyadevan, B.; Hashida, T.; Tohji, K. *ACS Nano* **2008**, *2*, 348–356.
(2) Endo, M.; Muramatsu, H.; Hayashi, T.; Kim, Y. A.; Van Lier, G.; Charlier, J. C.; Terrones, H.; Terrones, M.; Dresselhaus, M. S. *Nano Lett.* **2005**, *5*, 1099–1105.
(3) Lowell, C. E. *J. Am. Ceram. Soc.* **1967**, *50*, 142–144.
(4) Murty, H. N.; Biederman, D. L.; Heintz, E. A. *Fuel* **1997**, *56* 305–312.
(5) Miyazaki, K.; Hagio, T.; Kobayashi, K. *J. Mater. Sci.* **1981**, *16*, 752–762.
(6) Hagio, T.; Ogawa, I.; Kobayashi, K. *J. Mater. Sci.* **1986**, *21* 4147–4150.
(7) Hagio, T.; Nakamizo, M.; Kobayashi, K. *Carbon* **1989**, *27* 259–263.
(8) Park, S.; Srivastava, D.; Cho, K. *Nano Lett.* **2003**, *3*, 1273–1277.
(9) Lu, X.; Chen, Z. F.; Schleyer, P. R. *J. Am. Chem. Soc.* **2005**, *127*, 20–21.
(10) Rome-Herrera, J. M.; Terrones, M.; Terrones, H.; Dag, S.; Meunier, V. *Nano Lett.* **2007**, *7*, 570–576.
(11) Iwashita, N.; Park, C. R.; Fujimoto, H.; Shiraishi, M.; Inagaki, M. *Carbon* **2004**, *42*, 701–714.
(12) Rich, R. L. Boron though Thallium, the Triels. In *Inorganic Reactions in Water*; Springer: Berlin, 2007; p 309.
(13) Lay, L. Chemical Properties of Ceramics−Comparative Tables. In *Corrosion Resistance of Technical Ceramics*, 2nd ed.; HMSO: London, 1991; pp 105−151.
(14) Han, W.; Bando, Y.; Kurashima, K.; Sato, T. *Appl. Phys. Lett.* **1998**, *73*, 3085–3087.
(15) Serina, V.; Brydsonb, R.; Scottb, A.; Kihna, Y.; Abidatea, O.; Maquin, B.; Derre, A. *Carbon* **2000**, *38*, 547–554.
(16) McGuire, K.; Gothard, N.; Gai, P. L.; Dresselhaus, M. S.; Sumanasekera, G.; Rao, A. M. *Carbon* **2005**, *43*, 219–227.
(17) Please reference JCPDS card. $Al_5(BO_3)O_6$: No. 34−1039; B_4C: No. 35−0798.
(18) Tuinstra, F.; Koenig, J. L. *J. Chem. Phys.* **1970**, *53*, 1126–1130.
(19) Nemanich, R. J.; Solin, S. A. *Phys. Rev. B* **1979**, *20*, 392–401.
(20) Vidano, R. P.; Fischbach, D. B.; Wills, L. J.; Loehr, T. M. *Solid State Commun.* **1981**, *39*, 341–344.
(21) Chieu, T. C.; Dresselhaus, M. S.; Endo, M. *Phys. Rev. B* **1982**, *26*, 5867–5877.
(22) Wang, Y.; Alsmeyer, D. C.; McCreery, R. L. *Chem. Mater.* **1990**, *2*, 557–563.
(23) Hishiyama, Y.; Irumano, H.; Kaburagi, Y. *Phys. Rev. B* **2001**, *63*, 245406.